ACS APPLIED ENERGY MATERIALS

www.acsaem.org

Article

Microagglomerate of VO_2 Particles Packing Paraffin Wax Using Capillary Force as a Latent Thermal Energy Storage Medium

Kazuma Isobe,* Kaketo Yamauchi, Yutaka Yamada, and Akihiko Horibe

Cite This: *ACS Appl. Energy Mater.* 2025, 8, 9595−9603

Read Online

ACCESS | Metrics & More | Article Recommendations | Supporting Information

ABSTRACT: This study proposed a material to retain paraffin wax with vanadium dioxide (VO_2) particles as a latent thermal energy storage medium, an alternative to core−shell microcapsules containing phase change materials. VO_2 microparticles, which were synthesized through a sol−gel method and annealing process, were dispersed in the oil-in-water microemulsion to obtain microagglomerates of VO_2 microparticles. The average diameter of microagglomerates was 5 μm, and they retained paraffin wax at the vacancies among VO_2 particles. Although the microagglomerates had no complete shells similar to core−shell microcapsules, the microagglomerates successfully trapped paraffin wax droplets without any leakage even in a high-temperature environment. It was because capillary forces acting among VO_2 particles strictly prevented any leakage of paraffin waxes. The differential scanning calorimetry revealed that the microagglomerates contained only 16.5 wt % of *n*-octadecane, used as a paraffin wax. However, since VO_2 particles can release or absorb latent heat due to their metal−insulator phase transition, the proposed microagglomerates exhibited higher thermal energy storage densities than phase change microcapsules whose shells do not show phase transitions. Moreover, the microagglomerates exhibited higher thermal conductivity than microcapsules with amorphous inorganic shells because the VO_2 particles were crystallized through annealing. The proposed microagglomerate is a promising form for further improving the thermal energy storage density and thermal performance of the latent thermal energy storage medium, especially in the temperature range of 30 to 70 °C.

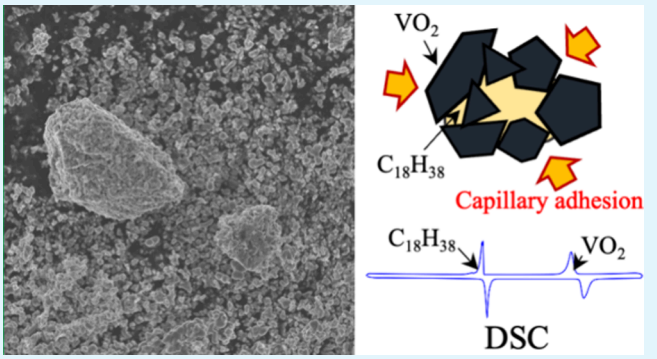

KEYWORDS: *microagglomerate, vanadium dioxide, paraffin wax, latent thermal energy storage medium, capillary force, thermal energy storage density, thermal conductivity*

1. INTRODUCTION

Improving the thermal efficiency of systems is a critical issue in reducing the consumption of fossil fuels and achieving low carbon emissions. Thermal energy storage techniques have been drastically improved within a few decades to utilize wasted thermal energy inevitably generated in industries.[1] Moreover, thermal energy storage also plays an important role in improving the overall efficiency of solar energy collectors.[2] Since large parts of solar radiation energy dissipate as heat during the solar photovoltaic power generation process, photovoltaic-thermal collectors have been proposed for thermal and electrical cogeneration.[3] Among thermal energy storage techniques, latent thermal energy storage is a promising technology that applies the latent heat released or absorbed during the solid−liquid or solid−solid phase change of materials. Latent energy storage has a higher energy storage density compared to sensible heat energy storage, and it is much more stable than chemical energy storage. Representative candidates of phase change materials (PCMs) are water-ice,[4] paraffin waxes,[5,6] fatty acids,[5,7] and sugar alcohols.[8,9] These are suitable for thermal energy storage at temperatures below 200 °C. The demand for thermal management in the temperature range of 30 to 70 °C is increasing in factories, artificial satellites, and electronic devices, among others. Consequently, considerable studies on these PCMs have been conducted.[10,11] Moreover, inorganic salt hydrates[12] and melting metals[13] are utilized at temperatures higher than 300 °C.

When PCMs are used as heat transfer fluid in practical thermal systems, they are usually microencapsulated with shell materials to ensure the flowability of PCMs in both liquid and solid phases.[1] Therefore, the slurry of microencapsulated PCMs is easier to handle and has a higher heat transfer area than nonencapsulated PCMs. Furthermore, the shells of microcapsules prevent leakages of flammable PCMs, such as

Received: April 28, 2025
Revised: June 10, 2025
Accepted: June 10, 2025
Published: June 16, 2025

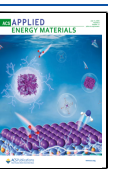

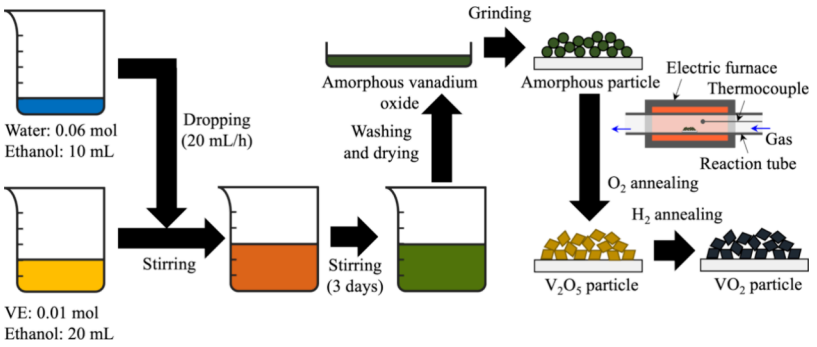

Figure 1. Preparation process of VO_2 particles through a sol−gel method.

paraffin and sugar alcohols, into the thermal system. Poly(methyl methacrylate),[14] melamine-formaldehyde resin,[15] and polystyrene[16] are representative shells made of organic materials. Although microcapsules with organic shells have economic advantages, they have disadvantages in flammability and thermal conductivity. Thermal conductivity plays a crucial role in enhancing the thermal regulation and thermal energy storage performances during the melting and solidification cycles. Silicon dioxide,[8,17] titanium oxide,[18] aluminum oxide,[13] and calcium carbonate[19] are notable candidates for inorganic shells with relatively high thermal conductivity. Generally, when inorganic shells encapsulate dispersed PCMs, precursor molecules for the shell materials are attracted around PCMs and polymerize to form core−shell structures through sol−gel[8,17] or self-assembly[18,19] processes. The encapsulation process via the Pickering emulsion state, using microparticles instead of precursors, also has the potential to provide unique characteristics to shells.[20] However, these shell materials occasionally suppress thermal energy storage density because the shell materials usually release or absorb no latent heat. Therefore, synthesizing thin and stable shells to improve the encapsulation ratio of PCMs is one of the critical issues for microcapsules.

Recently, vanadium dioxide (VO_2) has taken researchers' attention as a functional solid material with unique characteristics, which is beneficial to improving the performance of latent storage media. VO_2 is a metal−insulator transition (MIT) material exhibiting a solid−solid crystal phase change with latent heat. VO_2 shows metallic conductivity and optical reflectivity at a temperature higher than 68 °C, while it shows glass-like insulating and transparent properties at a low temperature. Therefore, numerous researchers applied VO_2 for passive control of optical properties.[21] The latent heat during the MIT is also remarkable, especially in space engineering, because of the stability, repeatability, and high thermal energy storage density of VO_2.[22] Guo et al. proposed a nanofiber made of a series of VO_2 nanoparticles for promoting thermal reallocation.[23] Several researchers proposed microcapsules containing VO_2 and paraffin waxes as PCMs.[24−26] Especially, Cheng et al. prepared tungsten- or tellurium-doped VO_2 nanoparticles and encapsulated paraffin waxes using prepared VO_2 nanoparticles.[25] Here, the MIT temperature of doped VO_2 decreases with increasing dopant concentration.[27] Therefore, the MIT temperatures were manipulated to the same temperature as the phase change temperatures of paraffin to enhance latent heat at one phase change temperature. Because of the latent heat from both cores and shells, the VO_2 microcapsules had higher energy storage density than other microcapsules.

Since amorphous vanadium oxide does not exhibit MIT, annealing treatments at 400 °C are required to obtain crystallized VO_2 from amorphous one. Although paraffin can be directly encapsulated by amorphous vanadium oxide through a sol−gel method, paraffin evaporates and breaks vanadium oxide shells during the annealing treatment. Therefore, researchers have tried to form spherical microcapsules using precrystallized VO_2 nanoparticles. Here, the essential point is to capture core materials inside the shell materials without leakage, while a capsule-like spherical appearance, as reported in past studies, is not mandatory.[23] Based on this point, we propose an alternative form to sustain paraffin waxes stably, a microagglomerate, aiming to utilize it as a latent energy storage medium at temperatures ranging from 30 to 70 °C. In this study, we synthesized microagglomerates containing VO_2 particles that stably capture paraffin waxes utilizing capillary forces among particles. Moreover, the thermophysical properties of the microagglomerates were assessed to evaluate their thermal energy storage performance and durability.

2. METHODOLOGY

2.1. Reagents. To fabricate micrometer-sized VO_2 particles, vanadium triethoxideoxide (VE) (Kojundo Chemical Laboratory Co. Ltd., Japan) was used as a precursor. Pure water purchased from Fujifilm Wako Pure Chemicals Corp., Japan, was used to proceed with the polymerization reaction of the precursor. Ethanol with 99.5% purity (Fujifilm Wako Pure Chemicals Corp., Japan) was used as a solvent. As a core material, *n*-octadecane ($C_{18}H_{38}$) with 99% purity (Thermo Fisher Scientific, USA), a kind of paraffin wax, was used in this study. Although the phase change and MIT temperatures of *n*-octadecane and undoped VO_2 are different, the temperature difference is beneficial for demonstrating the existence of both materials inside the microagglomerates. Cetyltrimethylammonium bromide (CTAB) (Fujifilm Wako Pure Chemicals Corp., Japan) was used as a cationic surfactant. As a referential sample for thermal analysis, commercialized VO_2 particles (Kojundo Chemical Laboratory Co. Ltd., Japan) were also prepared. Notably, the commercialized VO_2 particles were not applied for microagglomerate fabrication because the average diameter was too large.

2.2. VO_2 Particle Preparation. The VO_2 particles used in this study were synthesized using a sol−gel method. Figure 1 shows a schematic diagram of the fabrication process. First, 0.01 mol of VE was dissolved into 20 mL of ethanol. Second, 10 mL of ethanol with 0.06 mol of pure water was added to the

https://doi.org/10.1021/acsaem.5c01241
ACS Appl. Energy Mater. 2025, 8, 9595−9603

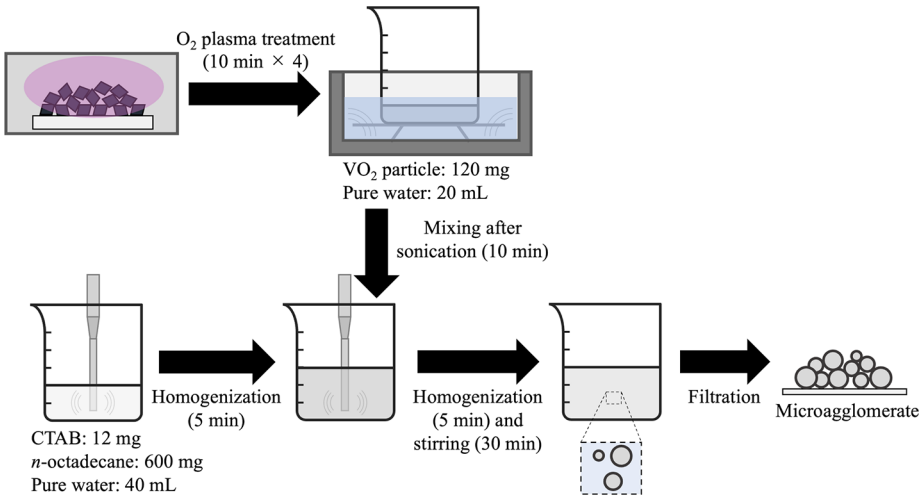

Figure 2. Synthesis process of *n*-octadecane@VO_2 microagglomerates using VO_2 particles.

VE solution with stirring. Here, VE and water cause hydrolysis and condensation reactions as follows:

$$VO(OC_2H_5)_3 + H_2O \rightarrow VO(OC_2H_5)_2OH + C_2H_5OH \quad (1)$$

$$2VO(OC_2H_5)_2OH \rightarrow O(VO(OC_2H_5)_2)_2 + H_2O \quad (2)$$

Hydroxy groups substitute ethoxy groups in turn to proceed with polymerization. However, since hydrolysis and condensation reactions progress quickly, a large amount of water sometimes prevents an ideal polymerization reaction among VE molecules. Therefore, the drop rate of the ethanol−water mixture was controlled mechanically at 20 mL/h using a syringe pump (YSP-201; YMC Co. Ltd., Japan) to slow the hydrolysis reaction. The solution was stirred for 3 days at room temperature to promote the polymerization of VE. The color of the VE solution gradually changed from orange to green with the progress of the polymerization reaction. The green solution was washed with ethanol and centrifuged several times to remove unreacted residues. Then, amorphous vanadium oxide was obtained after drying the VE solution. The dried amorphous vanadium oxide was strongly ground in a mortar made of alumina using a pestle to obtain particulate vanadium oxide. This grinding process works to separate agglomerated particles. The amorphous particles were annealed in a tubular electric furnace under an oxygen environment for 60 min to obtain crystallized V_2O_5 particles. The furnace temperature was at 400 °C, measured using a thermocouple inserted into the reaction tube made of fused silica. The V_2O_5 particles were also reduced at 400 °C under a hydrogen and argon mixed environment for 50 min to obtain VO_2 particles. The partial pressures of hydrogen and argon were respectively 14 and 50 kPa. Finally, approximately 300 mg of VO_2 particles could be obtained.

2.3. Microagglomerate Preparation. In this study, we fabricated microagglomerates with reference to a self-assembly method, which is usually used to synthesize core−shell microcapsules. In the general self-assembly method, surfactants are dispersed on the surface of core PCMs to attract precursor molecules of shell material by Coulomb forces.[19] Instead of liquid precursors, we used crystallized VO_2 particles. Figure 2 shows the synthesis process of microagglomerates using VO_2 particles. First, the surface of VO_2 particles was modified to be a hydrophilic surface using an O_2 plasma modifier (PM100; Yamato Scientific Co. Ltd., Japan). For sufficient modification, we repeated the plasma treatment and stirring process four times. Second, an ultrasonic cleaner dispersed 120 mg of modified VO_2 particles in 20 mL of pure water solvent. Simultaneously, 12 mg of CTAB and 600 mg of *n*-octadecane were mixed with 40 mL of pure water solvent at 60 °C. The solution was sonicated for 5 min using an ultrasonic homogenizer (SONICSTAR85; AS ONE Corp., Japan) at a power of 80 W to make an oil-in-water microemulsion. Third, the solution with VO_2 particle was added to the microemulsion. Since the surface of VO_2 particles tends to be charged negatively after plasma treatment,[28] the hydrophilic bases of CTAB molecules with a positive charge attracted VO_2 particles around each oil droplet. Then, VO_2 particles captured the droplets of *n*-octadecane. The solution was kept sonicated for 5 min after adding VO_2 particles to reduce the average diameters of microagglomerates. After the sonication process, the solution was stirred at 60 °C for 30 min without using the ultrasonic homogenizer to stabilize the microagglomerates. Finally, *n*-octadecane@VO_2 microagglomerates were extracted through the suction filtration process. The microagglomerates were washed using additional distilled water at 60 °C during filtration to remove surplus *n*-octadecane and imperfect microagglomerates. Extracted microagglomerates were dried on a Petri dish for 1 day to evaluate thermal and morphological characteristics.

2.4. Characterization Methods and Equipment. To investigate the crystallinity of vanadium oxide particles before and after annealing treatment, X-ray diffraction (XRD) (SmartLab; Rigaku, Japan) was analyzed at room temperature.

The shape and surface morphology of VO_2 particles and microagglomerates were observed by the scanning electron microscope (SEM) (SU9000; Hitachi High-Tech Co., Japan) at an accelerating voltage of 10 kV. Moreover, internal cross sections of several microagglomerates were exposed through the focused ion beam (FIB) milling process and observed using the attached SEM (JIB-4500; JEOL Ltd., Japan). The accelerating voltage for the FIB-SEM observation was adjusted for each structural condition.

Differentiating scanning calorimetry (DSC) (DSC7000X, Hitachi High-Tech Science Co., Japan) was conducted to measure specific enthalpies from VO_2 and *n*-octadecane

https://doi.org/10.1021/acsaem.5c01241
ACS Appl. Energy Mater. 2025, 8, 9595−9603

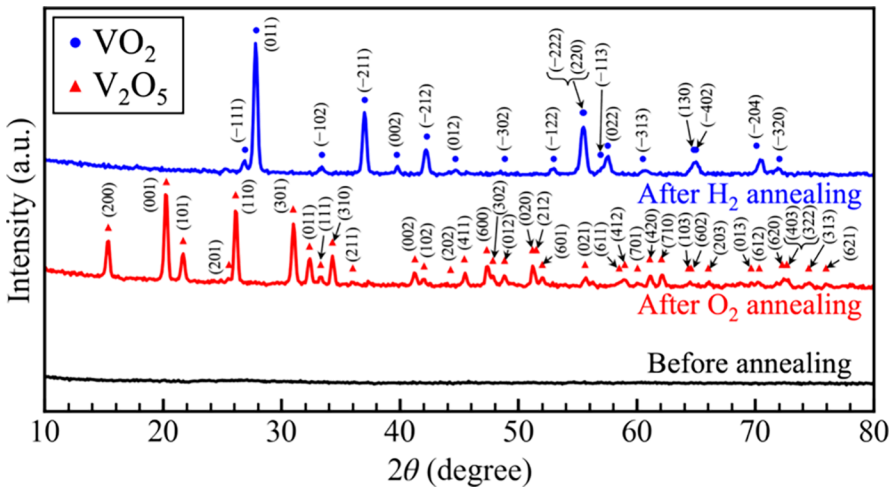

Figure 3. XRD patterns for the vanadium oxide particles. The blue and red dots express the major diffraction angles of VO_2 and V_2O_5, respectively, described in the PDF cards.

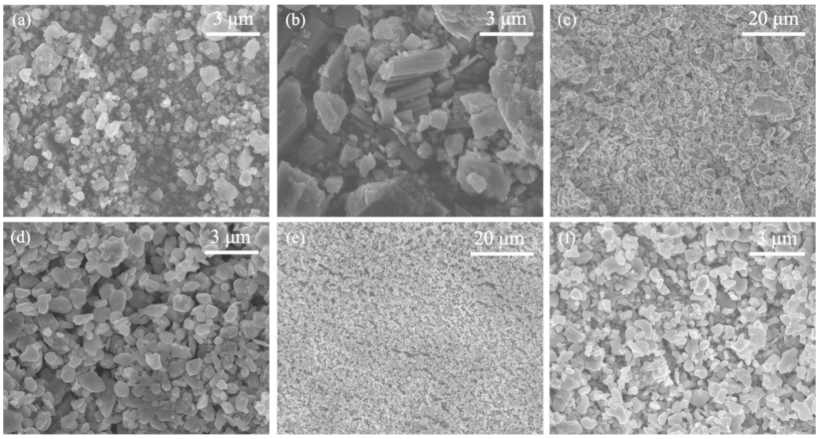

Figure 4. SEM images of (a) amorphous vanadium oxide and crystallized particles annealed at (b), (c) 500 °C and (d)-(f) 400 °C. (b) and (d) are snapshots after O_2 annealing, while (c), (e), and (f) are those after H_2 annealing.

associated with their phase change. The heating and cooling rates were set to be 10 °C/min for all measurements.

The effective thermal conductivities of synthesized microagglomerates were measured using a steady state comparative-longitudinal heat flow method.[29−31] First, the ends of two cylindrical stainless rods, whose diameters were 8 mm, were coated by a thin thermal grease layer. The microagglomerates were sandwiched by two rods to form a pellet. The two rods were set vertically on a cooling block and compressed at a constant pressure by an electric heater on the upper end of the rod. The upper/lower ends of rods were respectively maintained at 30 °C/10 °C during the measurement. The heat flux inside the two rods was calculated from the temperature gradient of the two rods, measured by ten thermocouples. Finally, the thermal conductivity of the pellet was derived from its thickness and heat flux.

The thermal durability of microagglomerates was evaluated visually and thermally. First, small lumps of both *n*-octadecane and microagglomerates were heated on the hot plate. The plate temperature was raised from 20 to 60 °C, which is higher than the melting point of *n*-octadecane, 28 °C. The shape and appearance of both samples were continuously recorded throughout the heating experiment. Second, the phase change enthalpies of microagglomerates that showed no leakage during and after the heating were repeatedly measured by the DSC. The cyclic measurement of DSC was conducted 100 times. Moreover, thermogravimetric analysis (TGA) (DTG-60, Shimadzu Corp., Japan) was conducted to quantitatively evaluate the thermal stability of the microagglomerate under the nitrogen atmosphere. The heating rate was set to be 10 °C/min.

3. SYNTHESIS RESULTS AND DISCUSSION

3.1. VO_2 Primary Particles. Figure 3 shows XRD analysis results for the vanadium oxide particles. Before annealing, raw vanadium oxide particles showed no peaks because they were amorphous. After annealing in an oxygen environment, the amorphous vanadium oxide transformed into V_2O_5 crystals. Therefore, the diffraction peak angles entirely correspond to the powder diffraction file (PDF) of No. 00−041−1426, which describes the diffraction pattern of orthorhombic V_2O_5 crystal with each orientation. The V_2O_5 particles changed their crystal structures after an appropriate duration of the reductive annealing. The XRD pattern of obtained particles matches the PDF of No. 00−019−1398, which describes the diffraction pattern of monoclinic VO_2 crystals. Additionally, no diffraction peaks originating from other crystals were observed. The XRD

https://doi.org/10.1021/acsaem.5c01241
ACS Appl. Energy Mater. 2025, 8, 9595−9603

result ensured that we could obtain crystallized VO_2 particles through the current synthesis process.

Figure 4 shows the SEM images of the vanadium oxide particles during the preparation process. Before conducting any annealing treatment, more than 90% of vanadium oxide particles had diameters less than 1 μm, as shown in Figure 4(a). Since the particles were sufficiently milled, particles were well separated from each other. In addition to the pregrinding for the particle, annealing temperature affected the diameter of VO_2 particles. Figure 4(b) shows the SEM image of the vanadium oxide particles after annealing at 500 °C with O_2 gas. Although the ambient temperature in the furnace was at 500 °C, the surface temperature of V_2O_5 particles during oxidative annealing possibly reached 690 °C, which is the melting point of V_2O_5. It was because the V_2O_5 particles received infrared rays from the heating wire in the electric furnace. Therefore, V_2O_5 particles melted during the annealing process and recrystallized among nearby particles, forming grains larger than 10 μm in size. The melted V_2O_5 particles could not reduce their size spontaneously even after recrystallization as VO_2 particles through annealing with H_2 gas. Eventually, the VO_2 particles obtained through annealing at 500 °C also exhibited relatively large grains, as shown in Figure 4(c). On the other hand, the V_2O_5 particles kept their original sizes with oxidative annealing at 400 °C, as shown in Figure 4(d). Figures 4(e) and 4(f) show the SEM images of VO_2 particles after the reductive annealing. While the average diameter was relatively small, the average sphericity of VO_2 particles was low because of their monoclinic crystal structure. In this study, VO_2 particles with average diameters less than approximately 1 μm were used for assembling agglomerates with smoother appearances.

3.2. Microagglomerates. Figure 5 shows the SEM images of the microagglomerates synthesized in this study. Several

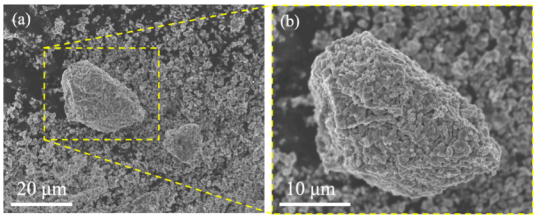

Figure 5. SEM images of *n*-octadecane@VO_2 microagglomerates. The microagglomerate surrounded by dashed lines in (a) is magnified as (b).

thousands of VO_2 particles assembled distorted agglomerates with diameters of 10 to 30 μm. The particles were stacked over a few layers to form stair-like surface morphology. Since CTAB molecules distributed on the surface of *n*-octadecane attracted VO_2 particles by Coulomb forces, the particles precisely covered *n*-octadecane droplets. However, the sphericity of observed microagglomerates was not high, similar to that of VO_2 particles, despite the spherical shapes of *n*-octadecane droplets during sonication. One reason was the randomness of VO_2 particles' shapes and diameters. The *n*-octadecane droplet adjusted its shape to minimize the interfacial free energy when the droplet attracted VO_2 particles at the water−oil interface. Attracted VO_2 particles with various shapes physically interfered with nearby particles, and the droplet needed further adjustment of its shape. Therefore, the true sphere could not be the best shape for the microagglomerate to reduce the interfacial free energy. Another reason was the unifications of *n*-octadecane droplets after sonication. The average diameter of *n*-octadecane droplets during sonication was less than 1 μm while droplets gradually unified with nearby droplets and enlarged until several microns after stopping sonication. Several droplets could unify with another droplet containing VO_2 particles, which caused complicated physical interferences. As a result, several microagglomerates grew distorted shapes and had diameters of 30 μm.

Figure 6 shows SEM observation results for microagglomerates during the FIB milling process. Figure 6(a)

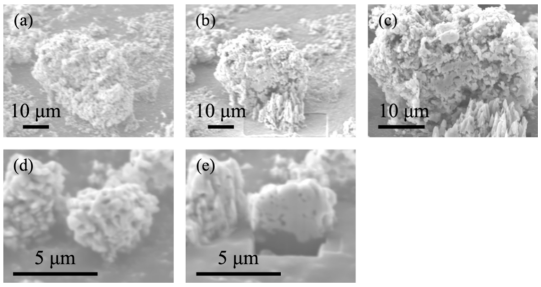

Figure 6. SEM images of microagglomerates before and after FIB treatments at accelerating voltages of (a), (b) 5 kV, (c) 15 kV, and (d), (e) 10 kV. (c) is a magnified view of (b) at the same view angle.

depicts the external appearance of a microagglomerate with a diameter of approximately 40 μm. As shown in Figures 6(b) and 6(c), a part of the microagglomerate was milled using FIB to reveal the inside morphology. The cross-section inside the microagglomerate showed a nonuniform framework. While smooth cross-sectional surfaces of agglomerated particles were observed, micrometer-sized vacancies surrounded the smooth surfaces. The average diameter of the smooth surface was approximately 5 μm, and the vacancies among primary particles were almost filled. Figures 6(d) and (e) show the external and internal appearances of a microagglomerate with a diameter of less than 5 μm. The cross-section of the small microagglomerate showed a higher uniformity than the large microagglomerate, and vacancies were comparably small. The uniform cross-section of the small microagglomerate implies that the large microagglomerates were the aggregations of tiny agglomerates with diameters of less than 5 μm. These tiny agglomerates gradually unified to form large agglomerates when the emulsion with agglomerates were stirred.

Although the SEM images minutely describe the microagglomerate morphology, we could not clearly distinguish the occupying domains for VO_2 particles and *n*-octadecane from the SEM images. Instead of the SEM observation, thermal analysis ensured *n*-octadecane existed around VO_2 particles. Figure 7 shows the DSC profile of the *n*-octadecane@VO_2 microagglomerate, *n*-octadecane, and VO_2 particle samples. The profiles are the results from the second cycle of each cyclic DSC operation. The microagglomerate generated or absorbed heat at two temperatures corresponding to the phase change and MIT temperatures of *n*-octadecane and VO_2. Since the microagglomerate exhibited a non-negligible amount of phase change enthalpy of *n*-octadecane, a reasonable amount of *n*-octadecane should be observed in the cross-sectional view of microagglomerates.

Figure 8 describes a probable timeline of the packing mechanism. When the VO_2 particles were added to the oil-in-water emulsion, CTAB molecules attracted the VO_2 particles

https://doi.org/10.1021/acsaem.5c01241
ACS Appl. Energy Mater. 2025, 8, 9595−9603

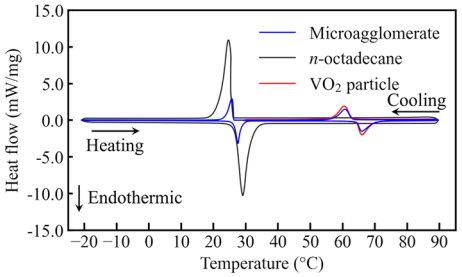

Figure 7. DSC curves for the *n*-octadecane@VO_2 microagglomerate and reference samples.

close to the oil−water interface due to the Coulomb force. However, the surfaces of the VO_2 particles were fundamentally hydrophilic and oleophobic. Therefore, the contact angle on the VO_2 surface for water, θ_{aq}, became smaller than that for oil, θ_o, at the capillary between two VO_2 particles. Moreover, the capillary force acting on the VO_2 surface side of the three-phase boundary tried to shut the capillary. As a result, two VO_2 surfaces made contact physically like a capillary adhesion. Of course, several submicron-sized capillaries should remain around the physical contact, but they were too narrow for paraffin waxes to leak out at room temperature. Eventually, the smooth cross-sectional surfaces observed in Figure 6 were mixtures of VO_2 particles and *n*-octadecane. Aggregation of VO_2 particles trapped *n*-octadecane within the vacancies among particles to form the microcapsule-like agglomerates. Therefore, "micro-agglomerate" would better describe the material of interest than "microcapsule."

4. THERMAL PERFORMANCE EVALUATION

Table 1 summarizes the thermophysical properties of each sample calculated from the DSC profiles shown in Figure 7. Table 1 also displays the properties of commercialized VO_2 particles as a reference. Here, T_m/T_s is the melting/solidification temperature of *n*-octadecane, $\Delta H_m/\Delta H_s$ is the phase change enthalpy per unit mass of *n*-octadecane, $T_{MI,h}/T_{MI,c}$ and $\Delta H_{MI,h}/\Delta H_{MI,c}$ are respectively the MIT temperature and enthalpy per unit mass of VO_2 during the heating/cooling procedure. The VO_2 particle synthesized in this study exhibited 80% of MIT enthalpy of the commercialized one. The suppression of the enthalpy was due to the remaining hydrocarbon group generated during the sol−gel process. Fortunately, no meaningful degradations in phase change and MIT temperatures were observed after the packing, as the packing process proceeded without any chemical reactions. In addition, *n*-octadecane could change its phase as usual even if it was trapped inside submicron-sized vacancies among VO_2 particles. However, the phase change enthalpy per unit mass of *n*-octadecane in the microagglomerate was much smaller than that of the pure *n*-octadecane. Since the density of VO_2 is approximately 5 times larger than that of *n*-octadecane, the difference in density resulted in a significant decrease in enthalpy.[32,33]

According to the latent heat observed from the micro-agglomerates, the mass fractions of *n*-octadecane and VO_2 in the microagglomerates, $E_{m,o}$ and E_{m,VO_2}, are calculated using the following formula:

$$E_{m,o} = \frac{\Delta H_{m,MA} + \Delta H_{s,MA}}{\Delta H_{m,o} + \Delta H_{s,o}} \quad (3)$$

$$E_{m,VO_2} = \frac{\Delta H_{MI,h,MA} + \Delta H_{MI,c,MA}}{\Delta H_{MI,h,VO_2} + \Delta H_{MI,c,VO_2}} \quad (4)$$

where, the subscripts o, VO_2, and MA respectively denote *n*-octadecane, VO_2, and microagglomerate. The mass fractions of *n*-octadecane and VO_2 were respectively 0.165 and 0.772; thus, those of other components, such as CTAB, were slightly remaining in the microagglomerates.

Table 2 shows the total phase change enthalpies per unit volume, ΔH_{total}, obtained by multiplying the densities of each sample by average enthalpies per unit mass. For calculating ΔH_{total}, the density of the microagglomerates, ρ_{MA}, was estimated as follows:

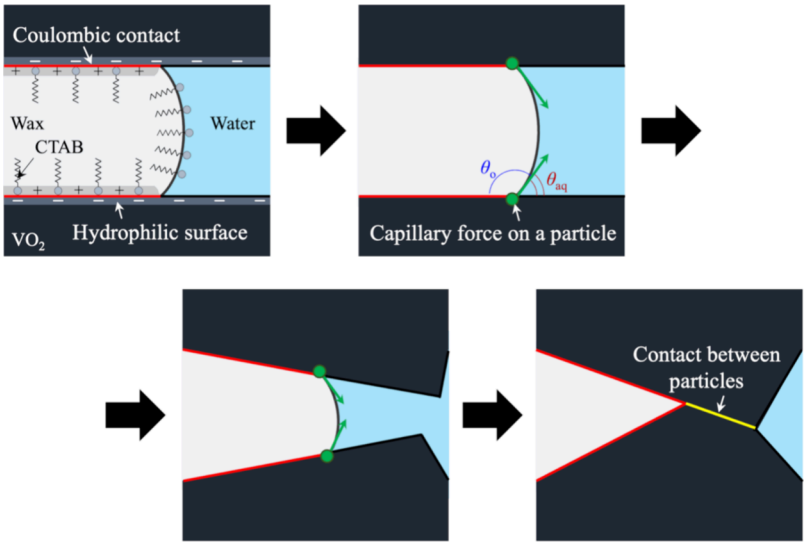

Figure 8. Schematic images around three-phase boundary among paraffin wax, VO_2, and water before the formation of microagglomerates.

https://doi.org/10.1021/acsaem.5c01241
ACS Appl. Energy Mater. 2025, 8, 9595−9603

Table 1. Phase Change Temperatures and Enthalpies per Unit Mass of *n*-octadecane, VO_2, and Synthesized Microagglomerates

	T_m (°C)	ΔH_m (mJ/mg)	T_s (°C)	ΔH_s (mJ/mg)	$T_{MI,h}$ (°C)	$\Delta H_{MI,h}$ (mJ/mg)	$T_{MI,c}$ (°C)	$\Delta H_{MI,c}$ (mJ/mg)
n-octadecane	29.06	240	24.67	237				
VO_2 particle (purchased)					67.25	56.2	61.35	55.6
VO_2 particle (this study)					66.03	44.5	60.55	44.6
microagglomerate	27.57	39.8	25.67	38.9	66.08	34.7	60.86	34.1

Table 2. Estimation of Total Phase Change Enthalpies per Unit Volume of *n*-octadecane, VO_2, and Synthesized Microagglomerates

	ΔH_{total} (J/cm^3)
n-octadecane	206
VO_2 particle (this study)	208
microagglomerate	207

$$\rho_{MA} = \left(\frac{\Delta H_{m,MA} + \Delta H_{s,MA}}{\rho_o(\Delta H_{m,o} + \Delta H_{s,o})} + \frac{\Delta H_{MI,h,MA} + \Delta H_{MI,c,MA}}{\rho_{VO_2}(\Delta H_{MI,h,VO_2} + \Delta H_{MI,c,VO_2})} \right)^{-1} \quad (5)$$

where, ρ_o (= 865 mg/cm^3 @20 °C) and ρ_{VO_2} (= 4670 mg/cm^3) are the densities of *n*-octadecane and VO_2 from the reference.[32,33] While the microagglomerate's phase change enthalpy per unit mass was much lower than that of *n*-octadecane, the microagglomerate had almost the same or slightly higher phase change enthalpy per unit volume because of VO_2. Here, the VO_2 particle synthesized in this study might have a lower density than the reference because of the remaining hydrocarbon group. Even in that case, the total phase change enthalpy per unit volume of the *n*-octadecane@VO_2 microagglomerate should be higher than that of microcapsules with shells showing no phase transition. Moreover, microagglomerate has potential to capture other paraffin waxes instead of *n*-octadecane. For example, microagglomerate with *n*-octacosane ($C_{28}H_{58}$), which has similar melting point to VO_2, is a suitable thermal energy storage medium around 65 °C.

Table 3 compares effective thermal conductivities of *n*-octadecane and latent storage media containing *n*-octadecane.

Table 3. Thermal Conductivity of *n*-octadecane, Microcapsule, and Microagglomerates

	k (W/(m K))
solid *n*-octadecane[34]	0.222
n-octadecane@silica[35]	0.151−0.621
n-octadecane@VO_2 (this study)	1.11 ± 0.01

Since VO_2 particles were well crystallized metal oxides, *n*-octadecane@VO_2 microagglomerate in this study exhibited higher thermal conductivity than microcapsules with inorganic shells. The high thermal conductivity of the shell is a remarkable advantage of microagglomerates consisting of metal oxide particles compared to capsules with amorphous shells.

Figure 9 shows snapshots of microagglomerate and *n*-octadecane during heating on the plate. A powder of microagglomerates was put on the right-hand side while a grain of *n*-octadecane was on the left-hand side. At 20 °C, the *n*-octadecane grain clearly showed its outline as solid. The grain gradually lost its shape as the temperature of the plate increased. Finally, at 60 °C, the grain completely melted and spread on the plate. However, the powder of microagglomerates showed no changes in appearance and no leakages during and after the heating experiment. This result guaranteed that VO_2 particles worked as thermally stable shells to prevent the leakage of *n*-octadecane in the atmospheric environment and water.

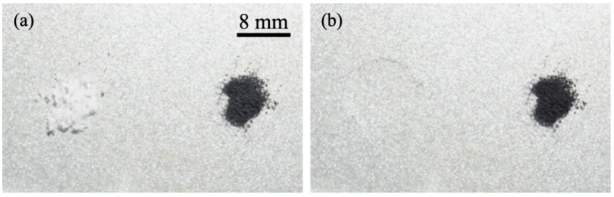

Figure 9. Snapshots during leakage test for the microagglomerates at (a) 20 °C and (b) 60 °C. The original video during this experiment is available as Video S1.

Figure 10 shows the result of the thermal durability test with cyclic DSC operations for the microagglomerates after the heating experiment. The DSC curve for the 100th cycle almost completely overlapped those for the first and 50th cycles. The microagglomerate exhibited no degradations in phase change temperatures and enthalpies for *n*-octadecane and VO_2. Therefore, this *n*-octadecane@VO_2 microagglomerate had good thermal reversibility, repeatability, and stability.

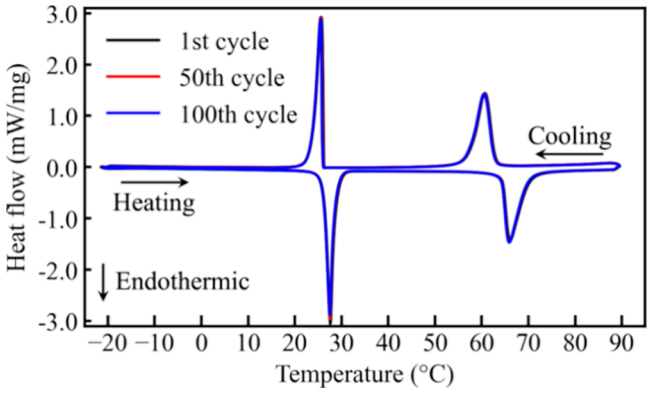

Figure 10. DSC curve for the *n*-octadecane@VO_2 microagglomerate during 100 times cyclic operations.

Figure 11 shows the result of the TGA experiment for the microagglomerate, which was the sample after conducting 100 cycles of the DSC measurement. Pure *n*-octadecane began to lose weight at approximately 130 °C and finished evaporation at 230 °C. VO_2 particles showed good thermal stability during the heating process. Desorption of water from the particle surface resulted in a slight weight reduction at approximately 100 °C. The microagglomerate exhibited a trend of weight reduction, like a combination of *n*-octadecane and VO_2 particles. Although the capillary force acting among VO_2

https://doi.org/10.1021/acsaem.5c01241
ACS Appl. Energy Mater. 2025, 8, 9595−9603

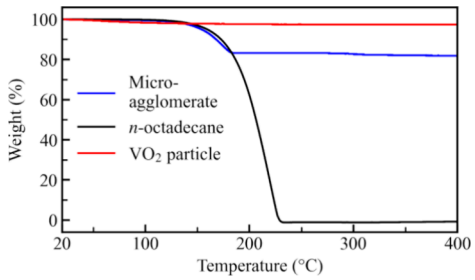

Figure 11. TGA curves for the *n*-octadecane@VO_2 microagglomerate and reference samples.

particles functioned to capture *n*-octadecane below 100 °C, the capillary force was insufficient to suppress the evaporation of *n*-octadecane over 130 °C. After the evaporation of *n*-octadecane, the microagglomerate lost 16.7% of its weight, which is consistent with the mass fraction ratio calculated from the DSC curves. Moreover, the microagglomerates exhibited further weight loss at around 300 °C, possibly due to a combustion reaction of the residual CTAB. Although the TGA experiment revealed a temperature limitation for the microagglomerate, this limitation is still acceptable for a latent thermal energy storage medium at temperatures ranging from 30 to 70 °C.

5. CONCLUSIONS

In this study, we proposed a microagglomerate stably containing paraffin wax as an alternative latent thermal energy storage medium for microcapsules. The microagglomerates consisted of *n*-octadecane, showing a solid−liquid phase change, and VO_2, showing a solid−solid phase change. Micrometer-sized VO_2 particles were added to the oil-in-water microemulsion to capture *n*-octadecane droplets. The surfactant molecules attracted VO_2 particles around the interface between *n*-octadecane and water by electrostatic forces. Here, the aggregation of VO_2 particles perfectly trapped the *n*-octadecane droplet inside the microagglomerate due to the capillary force acting between VO_2 particles. The primary microagglomerates had diameters less than 5 μm and often aggregated each other to form larger agglomerates. The DSC results showed that the obtained microagglomerate contained 16.5 and 77.2 wt % of *n*-octadecane and VO_2. Surprisingly, although the microagglomerates were not core−shell microcapsules with solid shells, the microagglomerates proved good thermal reversibility, repeatability, and stability below 100 °C. As a result, forming microagglomerates using crystallized VO_2 particles to capture paraffin waxes is a promising method to realize a latent thermal energy storage medium with high phase change enthalpies and thermal conductivity.

■ ASSOCIATED CONTENT

Supporting Information

The Supporting Information is available free of charge at https://pubs.acs.org/doi/10.1021/acsaem.5c01241.

Description of the supporting material (PDF)

Appearances of the microagglomerates and *n*-octadecane during the heating experiment (Video S1) (MP4)

■ AUTHOR INFORMATION

Corresponding Author

Kazuma Isobe − *Faculty of Environmental, Life, Natural Science and Technology, Okayama University, Okayama 700-8530, Japan;* orcid.org/0000-0002-8621-5015; Phone: +81-86-251-8048; Email: isobe.k.ad@okayama-u.ac.jp

Authors

Kaketo Yamauchi − *Graduate School of Environmental, Life, Natural Science and Technology, Okayama University, Okayama 700-8530, Japan*

Yutaka Yamada − *Faculty of Environmental, Life, Natural Science and Technology, Okayama University, Okayama 700-8530, Japan;* orcid.org/0000-0002-2823-6790

Akihiko Horibe − *Faculty of Environmental, Life, Natural Science and Technology, Okayama University, Okayama 700-8530, Japan*

Complete contact information is available at: https://pubs.acs.org/10.1021/acsaem.5c01241

Notes

The authors declare no competing financial interest.

■ ACKNOWLEDGMENTS

The authors would like to thank the Japan Society for the Promotion of Science (JSPS) KAKENHI Grant in Aide for Early-Career Scientists (Grant Number: JP22K14192) for their financial support. This work was also financially supported by the Taisei Foundation (Grant Number: 23003). We also acknowledge Dr. Hiroo Suzuki and Mr. Soma Kono for experimental support at Okayama University.

■ REFERENCES

(1) Jouhara, H.; Żabnieńska-Góra, A.; Khordehgah, N.; Ahmad, D.; Lipinski, T. Latent Thermal Energy Storage Technologies and Applications: A Review. *Int. J. Thermofluids* **2020**, No. 100039.

(2) Carmona, M.; Palacio Bastos, A.; García, J. D. Experimental Evaluation of a Hybrid Photovoltaic and Thermal Solar Energy Collector with Integrated Phase Change Material (PVT-PCM) in Comparison with a Traditional Photovoltaic (PV) Module. *Renew. Energy* **2021**, *172*, 680−696.

(3) Rejeb, O.; Gaillard, L.; Giroux-Julien, S.; Ghenai, C.; Jemni, A.; Bettayeb, M.; Menezo, C. Novel Solar PV/Thermal Collector Design for the Enhancement of Thermal and Electrical Performances. *Renew. Energy* **2020**, *146*, 610−627.

(4) Saito, A. Recent Advances in Research on Cold Thermal Energy Storage. *Int. J. Refrig.* **2002**, *25* (2), 177−189.

(5) Giro-Paloma, J.; Konuklu, Y.; Fernández, A. I. Preparation and Exhaustive Characterization of Paraffin or Palmitic Acid Microcapsules as Novel Phase Change Material. *Sol. Energy* **2015**, *112*, 300−309.

(6) Yang, R.; Li, D.; Salazar, S. L.; Rao, Z.; Arıcı, M.; Wei, W. Photothermal Properties and Photothermal Conversion Performance of Nano-Enhanced Paraffin as a Phase Change Thermal Energy Storage Material. *Sol. Energy Mater. Sol. Cells* **2021**, *219* (September 2020), No. 110792.

(7) Mjallal, I.; Feghali, E.; Hammoud, M.; Habchi, C.; Lemenand, T. Exploring the Colligative Properties of Arachidic Acid for Potential Use as PCM. *Sol. Energy* **2021**, *214* (November 2020), 19−25.

(8) Pethurajan, V.; Sivan, S.; Konatt, A. J.; Reddy, A. S. Facile Approach to Improve Solar Thermal Energy Storage Efficiency Using Encapsulated Sugar Alcohol Based Phase Change Material. *Sol. Energy Mater. Sol. Cells* **2018**, *185* (May), 524−535.

(9) Yu, J.; Horibe, A.; Haruki, N. Melting and Solidification Characteristic of Mixture of Two Types of Latent Heat Storage Material in Direct Contact Heat Exchanger. *Exp. Heat Transfer* **2024**, *38* (3), 224−244.
(10) Sharma, A.; Tyagi, V. V.; Chen, C. R.; Buddhi, D. Review on Thermal Energy Storage with Phase Change Materials and Applications. *Renew. Sustain. Energy Rev.* **2009**, *13* (2), 318−345.
(11) Elshaer, A. M.; Soliman, A. M. A.; Kassab, M.; Mori, S.; Hawwash, A. A. Thermal Control of a Small Satellite in Low Earth Orbit Using Phase Change Materials-Based Thermal Energy Storage Panel. *Egypt. J. Remote Sens. Sp. Sci.* **2023**, *26* (4), 954−965.
(12) Purohit, B. K.; Sistla, V. S. Inorganic Salt Hydrate for Thermal Energy Storage Application: A Review. *Energy Storage* **2021**, *3* (2), 1−26.
(13) Koide, H.; Kurniawan, A.; Takahashi, T.; Kawaguchi, T.; Sakai, H.; Sato, Y.; Chiu, J. N.; Nomura, T. Performance Analysis of Packed Bed Latent Heat Storage System for High-Temperature Thermal Energy Storage Using Pellets Composed of Micro-Encapsulated Phase Change Material. *Energy* **2022**, *238*, No. 121746.
(14) Zhang, G.; Cui, G.; Dou, B.; Wang, Z.; Goula, M. A. An Experimental Investigation of Forced Convection Heat Transfer with Novel Microencapsulated Phase Change Material Slurries in a Circular Tube under Constant Heat Flux. *Energy Convers. Manag.* **2018**, *171* (June), 699−709.
(15) Zhu, K.; Li, X.; Su, J.; Li, H.; Zhao, Y.; Yuan, X. Improvement of Anti-Icing Properties of Low Surface Energy Coatings by Introducing Phase-Change Microcapsules. *Polym. Eng. Sci.* **2018**, *58* (6), 973−979.
(16) Mohammadi, B.; Najafi, F. S.; Ranjbar, H.; Mohammadi, J.; Zakaryazadeh, M. Nanoencapsulation of Butyl Palmitate in Polystyrene-*Co*-Methyl Methacrylate Shell for Thermal Energy Storage Application. *Energy Build.* **2016**, *118*, 99−105.
(17) Okuno, K.; Isobe, K.; Horibe, A.; Yamada, Y. Synthesis and Characterization of Silica-Encapsulated *n*-Tetracosane and the Effect of Surface Modification by Silane Coupling Agents. *Int. J. Thermophys.* **2023**, *44* (5), 69.
(18) Chai, L.; Wang, X.; Wu, D. Development of Bifunctional Microencapsulated Phase Change Materials with Crystalline Titanium Dioxide Shell for Latent-Heat Storage and Photocatalytic Effectiveness. *Appl. Energy* **2015**, *138*, 661−674.
(19) Yamada, Y.; Sato, T.; Isobe, K.; Aly, W. I. A.; Horibe, A. Thermal Energy Storage Performance Enhancement of Microencapsulated *n*-Tetracosane with a Polymorph-Modulated Calcium Carbonate Shell. *Energy Fuels* **2023**, *37* (4), 3152−3158.
(20) Wang, H.; Zhao, L.; Chen, L.; Song, G.; Tang, G. Facile and Low Energy Consumption Synthesis of Microencapsulated Phase Change Materials with Hybrid Shell for Thermal Energy Storage. J. *Phys. Chem. Solids* **2017**, *111* (June), 207−213.
(21) Isobe, K.; Yamamoto, T.; Yamada, Y.; Horibe, A. Bayesian Optimization of Periodic Multilayered Slabs for Passive Absorptivity Control. *Int. J. Heat Mass Transfer* **2024**, *221* (November 2023), No. 125047.
(22) Yamagata, M. R.; Wakita, Y.; Tsuruda, Y.; Miyata, K. Feasibility Study of Low-Temperature Operable Electric Power Supply for CubeSats Using Passive Thermal Control with VO2-Based Solid−Solid Phase Change Material. *Therm. Sci. Eng. Prog.* **2023**, *37* (November 2022), No. 101601.
(23) Guo, H.; Si, L.; Yu, J.; Wang, X.; Si, Y. Phase-Engineered VO2 Meta Nanofiber Enables a Metal−Insulator Transition for Bidirectional Thermal Reallocation. *Nano Lett.* **2023**, *23* (13), 6233−6240.
(24) Zhang, X.; Long, Z. Preparation and Properties of Tungsten-Doped VO_2 Microcapsule Intelligent Temperature-Control Packaging Paper. *Prog. Org. Coat.* **2019**, *131* (February), 219−226.
(25) Cheng, T.; Wang, N.; Wang, H.; Sun, R.; Wong, C.-P. A Newly Designed Paraffin@VO_2 Phase Change Material with the Combination of High Latent Heat and Large Thermal Conductivity. *J. Colloid Interface Sci.* **2020**, *559*, 226−235.
(26) Wu, Y.; Liu, W.; Song, Z.; Yu, D.; Li, G.; Liu, X.; Wang, H. Paraffin Particle Dispersion Costabilized by W-Doped VO_2 Nanoparticles and Chitosan for the Fabrication of Functional Nanocellulose Film. *Appl. Surf. Sci.* **2022**, *604* (June), No. 154519.
(27) Wang, N.; Magdassi, S.; Mandler, D.; Long, Y. Simple Sol-Gel Process and One-Step Annealing of Vanadium Dioxide Thin Films: Synthesis and Thermochromic Properties. *Thin Solid Films* **2013**, *534*, 594−598.
(28) Émond, N.; Torriss, B.; Chaker, M. Natural and Induced Growth of VO_2 (M) on VO_2 (B) Ultrathin Films. *Sci. Rep.* **2018**, *8* (1), 7153.
(29) Ogushi, T.; Yanaura, S.; Watanabe, S.; Hirata, T. Thermal Conductivity Measurement Method for Isotropic Conductive Adhesives. *Netsu Bussei* **2015**, *28* (1), 22−28.
(30) Yamada, Y.; Horibe, A. Thermal Properties and Related Core/Shell Structure of n-Tetracosane Microencapsulated by Calcium Carbonate. *Appl. Therm. Eng.* **2020**, *178* (September 2019), No. 115512.
(31) Yamada, Y.; Nishiyama, T.; Yasuhara, T.; Takahashi, K. Thermal Boundary Conductance between Multi-Walled Carbon Nanotubes. J. Therm. *Sci. Technol.* **2012**, *7* (1), 190−198.
(32) Humphries, W. R.; Griggs, E. I. A Design Handbook for Phase Change Thermal Control and Energy Storage Devices. *NASA Technol. Rep.* **1977**, *255*, 15434.
(33) Alvarez-Guerrero, S.; Ordonez-Miranda, J.; de Coss, R.; Alvarado-Gil, J. J. Determination of the Effective Thermal Conductivity of Particulate Composites Based on VO2 and SiO2. *Int. J. Therm. Sci.* **2022**, *172* (PA), No. 107278.
(34) Li, J.; Mao, Y.; Yang, X.; Liao, Y. N.; Cai, D.; Chen, S. S.; Sun, K.; Zheng, Y. J. Molecular Dynamics Simulation of Thermal Properties of Modified Graphene/n-Octadecane Composite Phase Change Material. *J. Phys. Conf. Ser.* **2024**, *2749* (1), No. 012008.
(35) Zhang, H.; Wang, X.; Wu, D. Silica Encapsulation of n-Octadecane via Sol-Gel Process: A Novel Microencapsulated Phase-Change Material with Enhanced Thermal Conductivity and Performance. *J. Colloid Interface Sci.* **2010**, *343* (1), 246−255.

https://doi.org/10.1021/acsaem.5c01241
ACS Appl. Energy Mater. 2025, 8, 9595−9603